corrosion and materials degradation

MDPI

Article

Influence of Electrolytic Hydrogen Charging and Effusion Aging on the Rotating Bending Fatigue Resistance of SAE 52100 Steel

Johannes Wild, Stefan Wagner, Astrid Pundt and Stefan Guth *

Karlsruhe Institute of Technology (KIT), Institute for Applied Materials–Materials Science and Engineering (IAM-WK), 76131 Karlsruhe, Germany; johannes.wild@kit.edu (J.W.); stefan.wagner3@kit.edu (S.W.); astrid.pundt@kit.edu (A.P.)

* Correspondence: stefan.guth@kit.edu; Tel.: +49-721-608-42197

Abstract

Hydrogen embrittlement (HE) can significantly degrade the mechanical properties of steels. This phenomenon is particularly relevant for high-strength steels where large elastic stresses lead to detrimental localized concentrations of hydrogen at defects. In this study, unnotched rotating bending specimens of the bearing steel SAE 52100 (100Cr6) quenched and tempered at 180 °C and 400 °C were electrochemically charged with hydrogen. Charged and non-charged specimens then underwent rotating bending fatigue testing, either immediately after charging or after aging at room temperature up to 72 h. The hydrogen-charged specimens annealed at 180 °C showed a sizeable drop in fatigue limit and fatigue lifetime compared to the non-charged specimens with cracks mainly originating from near-surface non-metallic inclusions. In comparison, the specimens annealed at 400 °C exhibited a moderate drop in fatigue limit and lifetime due to hydrogen charging with cracks originating mostly from the surface. Aging had only insignificant effects on the fatigue lifetime. Notably, annealing of charged samples for 2 h at 180 °C restored their lifetime to that of non-charged specimens.

Keywords: hydrogen embrittlement; rotating bending fatigue; SAE52100; electrolytical hydrogen charging

Academic Editor: María Criado Sanz

Received: 22 May 2025
Revised: 2 July 2025
Accepted: 7 July 2025
Published: 9 July 2025

Citation: Wild, J.; Wagner, S.; Pundt, A.; Guth, S. Influence of Electrolytic Hydrogen Charging and Effusion Aging on the Rotating Bending Fatigue Resistance of SAE 52100 Steel. *Corros. Mater. Degrad.* **2025**, *6*, 30. https://doi.org/10.3390/cmd6030030

1. Introduction

It has been known for almost 150 years that interaction with hydrogen can drastically reduce the ductility and strength of structural steels, particularly when they exhibit high strength [1]. The effect is referred to as hydrogen embrittlement (HE). Numerous studies further showed that the cyclic properties of steels such as the fatigue lifetime and the fatigue limit, i.e., the stress amplitude a material can withstand for a specified number of cycles, may degrade under the influence of hydrogen [2–5]. This may be crucial in applications such as hydrogen storage tanks, which experience cyclic loads due to emptying and refilling or pipelines subject to oscillating pressures. However, there are also reports of positive hydrogen effects, e.g., for austenitic steels under bending fatigue loading [6,7]. Steels with higher initial strength degrade typically more under hydrogen influence [8]. Despite considerable research efforts, the mechanisms of hydrogen degradation of steels are still under debate [9]. For structural materials, which do not form hydrides, the hydrogen-enhanced decohesion theory (HEDE, also known as HID, hydrogen-induced decohesion) and the hydrogen-enhanced local plasticity (HELP) theory are considered as most viable [10,11].

The HEDE mechanism assumes that hydrogen reduces the cohesive energy along crystallographic planes, thus facilitating brittle fracture [12]. The HELP mechanism states that hydrogen promotes dislocation motion and thus plastic strain localization [13], which in turn reduces the fatigue strength [14]. Once monoatomic hydrogen has diffused into a metallic material, it may be trapped at open volume defects, e.g., inclusions, cracks, grain boundaries, retained austenite or dislocations [15–19]. The traps can be classified into reversible (shallow) traps acting as either sink or source of diffusible hydrogen and irreversible (deep) traps acting only as hydrogen sinks [15].

The hypereutectic steel SAE 52100 is typically applied in rolling bearings as rolling elements but also in highly loaded shafts. Both rolling elements and shafts may uptake hydrogen during production processes [20], during service in hydrogen-containing atmospheres, or through hydrogen-containing lubricants [21]. Karsch et al. and Ogawa et al. have shown that under tension-compression high frequency loading, the fatigue lifetimes as well as the fatigue limit in the high and very high cycle regime of SAE 52100 in martensitic state significantly reduce upon electrolytic hydrogen charging [8,22]. Both studies applied axial fatigue loading, where the stress amplitude is homogeneous throughout the volume and cracks initiated mainly subsurface. However, for typical shaft components subjected to rotating bending fatigue under hydrogen influence, the maximum stress amplitude occurs only at the surface, while the volume sees lower stress amplitudes. Since hydrogen diffusion will act also mainly near the surface, the lifetime of such shafts may be rather limited by surface crack initiation. With this study, we report on the influence of hydrogen charging on SAE 52100 under near service rotating bending fatigue. In addition to a standard heat treatment state annealed at 180 °C, we test also a softer state annealed at 400 °C. The soft state is expected to exhibit a lower dislocation density and thus a better resistance against hydrogen degradation. Further, we address the effects of hydrogen effusion on the fatigue resistance. Already, Johnson showed that a hydrogen-degraded material may restore its original properties upon aging at room temperature, which allows the hydrogen to effuse to the atmosphere containing a lower hydrogen partial-pressure [1]. Murakami et al. showed for a quenched and tempered steel SCM435 that continuous hydrogen effusion through aging at room temperature after charging restores the fatigue lifetime gradually [23]. Here, we investigate this behavior for SAE51200.

2. Materials, Specimens and Experimental Methods

Hypereutectoid steel SAE 52100 (100Cr6, JIS SUJ2) raw material was supplied in the form of rolled round bars with a diameter of 14 mm. Table 1 shows the chemical composition of the bars measured by optical emission spectroscopy. From the raw material, near-net-shape specimens were machined for the heat treatment, which consisted of austenitization at 850 °C (1123 K) for 20 min, oil-quenching to 60 °C and subsequent tempering for 120 min at either 180 °C (453 K) (treatment A) or 400 °C (673 K) (treatment B). After the heat treatment, the raw specimens were machined to the final dog-bone-shaped rotating bending fatigue specimens with a cylindrical gauge length of 30 mm with 7 mm diameter. The specimen geometry is shown in Figure 1. The gauge length surfaces were ground using a sequence of #1000, #2000 and #4000 grit silicon carbide and afterwards cleaned with acetone. After this finish, hardness profiles were measured across specimen cross sections that were prepared from the gauge lengths using a Vickers-type microhardness tester Qness Q10 A+ with an indentation load of 1 kg (HV 1.0). For each heat treatment state, three specimens were measured. The results are shown in Figure 2. For both treatments, the hardness is homogeneous across the gauge diameter, showing barely scatter, indicating that decarburization has not occurred during the heat treatment. The resulting mean hardness values were 789 $\pm$ 5 HV1 for treatment A and 587 $\pm$ 4 HV1 for treatment B. While treatment

A is a standard for SAE 52100 resulting in a martensitic microstructure, treatment B leads to a tempered microstructure, which was chosen because of the possibly higher resistance to hydrogen-induced degradation of the fatigue resistance due to the lower hardness [8]. For hydrogen content measurements after charging, 5 × 5 × 5 mm cube specimens were machined from the same bar material and heat-treated using the treatment B parameters. These samples then underwent the same grinding routine as the fatigue specimens.

Table 1. Chemical composition of the SAE52100 test material, given in wt. %.

C	Cr	Mn	Si	Cu	P	S	Fe
1.009	1.404	0.364	0.236	0.154	0.01	0.013	Bal.

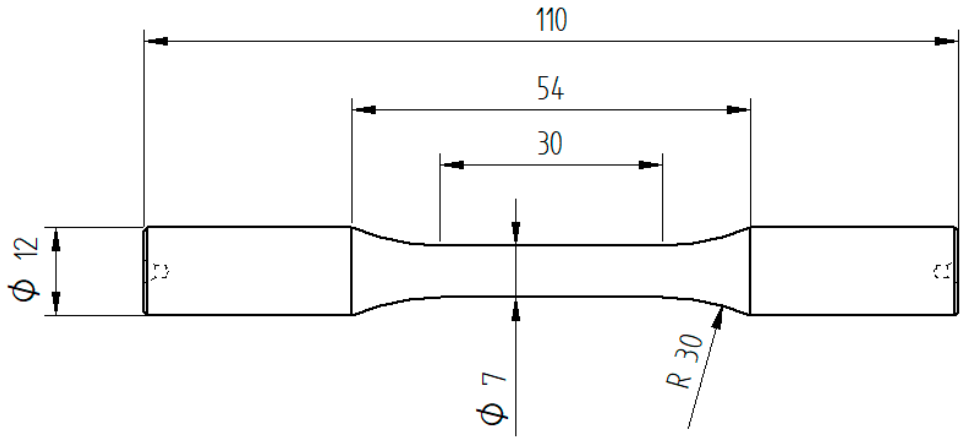

Figure 1. Specimen geometry used for rotating bending fatigue experiments. The dimensions are given in mm.

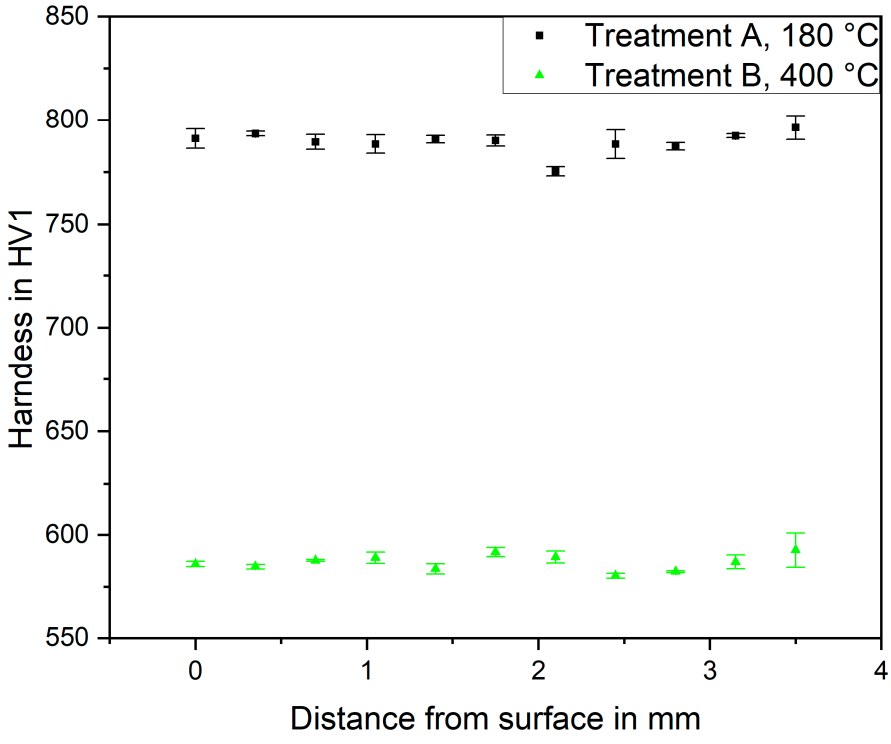

Figure 2. Mean hardness values measured on gauge length cross sections of rotating bending fatigue specimens as a function of the edge distance.

Hydrogen charging was performed cathodically with a precision current source meter of type 2601 by Keithely. The specimens were charged in an aqueous solution of 0.5-molar H_2SO_4 (sulphuric acid) using a platinum counter-electrode at a current density of 1.3 $\frac{mA}{cm^2}$ for 2 h at 20 °C. Details to the charging method can be, e.g., found in [8]. To avoid chemical attack of the specimens by the sulphuric acid solution, the current source was activated before placing the specimens in the electrolyte. In this way, the specimen was protected using impressed current cathodic protection. SEM observation did not show any visible damage on the specimen surfaces after charging. Using the hydrogen diffusion coefficient of hardened SAE 52100 at room temperature of $D_{eff} = 4.9 \times 10^{-12}$ m^2/s measured by Kürten et al. [24], the hydrogen penetration depth l after charging can be estimated by the one-dimensional Fick's law ($l = \sqrt{2D_{eff}\, t}$) resulting in l of the order of 250 µm for treatment A specimens. The diffusion coefficient of hydrogen in hardened steel alloyed with about 1 wt. % C increases by about an order of magnitude upon tempering at 400 °C [25]. Hence, for the treatment B specimens, the estimated hydrogen penetration depth should be of the order of 750 µm. In both cases, the hydrogen penetrates only the surface area of the gauge length, which corresponds to the subsequent rotating bending fatigue testing where the maximum stress occurs at the surface, while the core region sees only lower stresses.

The fatigue tests were conducted on a 100 Nm moment-controlled rotating bending machine at room temperature in laboratory air. The test setup is shown in Figure 3 and allows for loading with constant bending moments using a servoelectric motor and a force sensor. Owing to the rotating bending test setup, the tests were carried out at a load ratio of $R = -1$, i.e., with zero mean stress. The testing frequency was 50 Hz, which corresponds to a revolution speed of 3000 rpm. The maximum cycle number was set to 10^7 after which, in case no previous fracture occurred, the cycling was stopped and the specimens considered as runout. For the hydrogen-charged specimens, fatigue testing was started within 15 min after the charging process. Using the above-mentioned diffusion coefficients [24,25], the estimated hydrogen diffusion depth during 10^7 fatigue cycles (2×10^5 s, 55 h) is about 1.4 mm for state A, while for state B, it is larger than the specimen radius, i.e., full penetration. Further, effusion fatigue tests were conducted, where some specimens were deliberately aged at room temperature for 24, 48 and 72 h between hydrogen charging and fatigue testing.

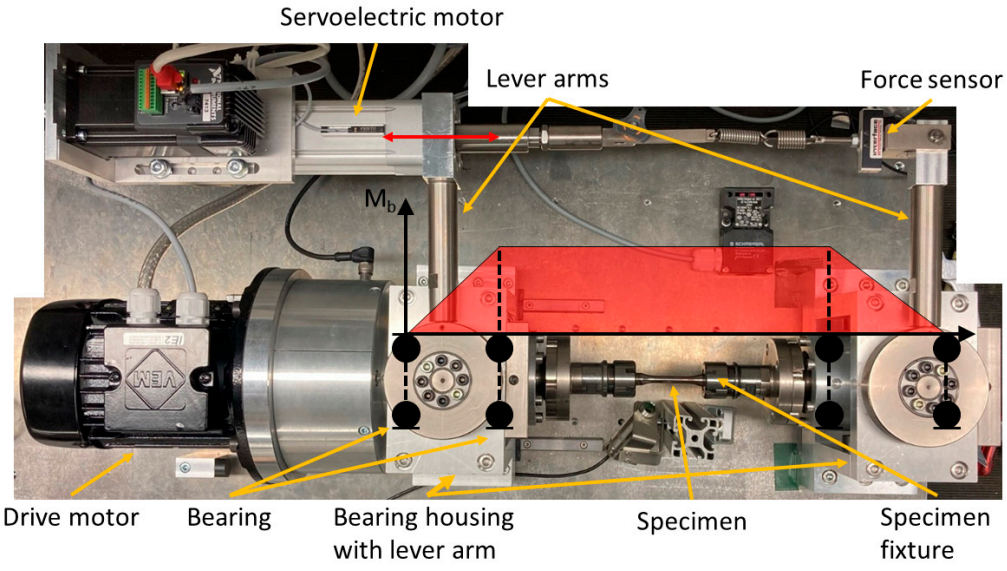

Figure 3. Rotating bending fatigue test setup. The bending moment is controlled via the servoelectric motor and the force sensor shown in the upper part of the image. The drive motor rotated at a speed of 3000 rpm resulting in a cycle frequency of 50 Hz.

The cube specimens for hydrogen content measurements were charged using the same parameters as for the fatigue specimens. The measurements were carried out on a G8 GALILEO ONH carrier gas hot extraction device by Bruker immediately either after charging or after different aging periods. Additionally, non-charged samples were tested in an ELEMENTRAC ONH device by Eltra to obtain the base level hydrogen content after manufacturing.

The fracture surfaces of the broken rotating bending fatigue specimens were investigated using a Zeiss Evo 50 scanning electron microscope (SEM) with an acceleration voltage of 20 kV.

3. Results and Discussion

Figure 4 shows the measured hydrogen content of SAE 52100 treatment B cube specimens in the non-charged state as well as hydrogen-charged for 2 h at 20 °C. The non-charged state showed hydrogen contents below 0.1 wppm, thus any further increase in hydrogen content is assumed to be due to the electrolytic hydrogen charging. The non-charged hydrogen content is lower than typical literature values of quenched and tempered SAE 52100, which are in the range of 0.6 to 0.7 wppm [8,26]. However, these values were derived for material tempered at temperatures around 200 °C, while the specimens measured here were tempered at 400 °C. Apparently, the hydrogen content from the as-hardened state effuses mostly during tempering at 400 °C, indicating that this content is either freely movable or reversibly trapped. This finding agrees well with thermal desorption measurements [27,28]. For the treatment A fatigue specimens, an initial hydrogen content in the range of 0.7 wppm can be assumed.

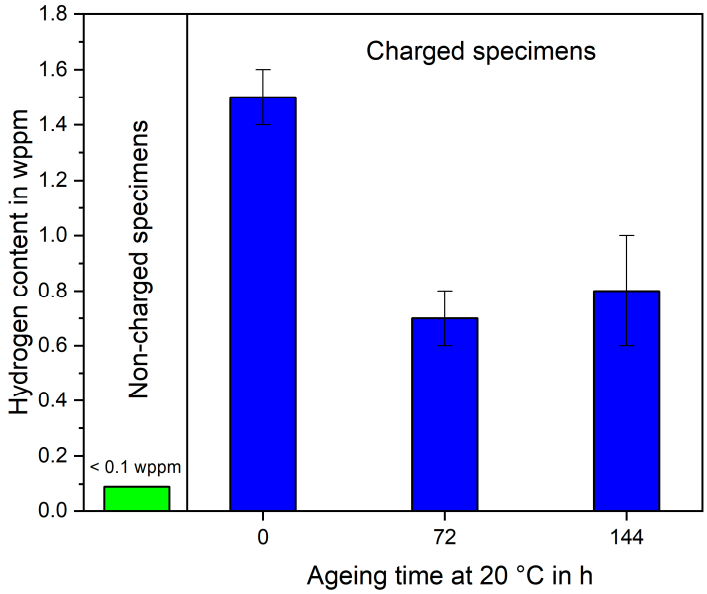

Figure 4. Total hydrogen content measured by carrier gas hot extraction in SAE 52100 cube specimens tempered for 120 min at 400 °C (treatment B), with and without subsequent aging at 20 °C.

Considering that the estimated penetration depth directly after charging is only about 250 µm for treatment A and 750 µm for treatment B, the effective local hydrogen content in the penetrated volume amounts to about 5.5 wppm and 2.25 wppm, respectively. After 72 h of aging, the estimated hydrogen penetration depth to the sample interior will cover more than 90% of the cube volume even for treatment A. Hence, for the charged and aged specimens, the measured and effective hydrogen content are nearly identical. The evolution of the hydrogen content during aging indicates a rather rapid effusion directly after charging followed by a stable state. A similar evolution was already reported by

Karsch et al. 2014 for the same material annealed at 180 °C (treatment A) [8]. Contrary to this, Murakami and Nagata observed a continuous decrease in hydrogen content for the quenched and tempered steel SCM435 [23]. Notably, the stable state hydrogen content in charged specimens after aging measured here is similar to that reported for non-charged SAE 52100 when annealed at temperatures around 200 °C [8,26]. This indicates that for a heat treatment at around 200 °C, the (at this temperature) sessile hydrogen content remains while all the mobile hydrogen is released.

Figure 5 shows the fatigue lifetimes dependent on stress amplitude for treatment A and treatment B specimens in non-charged and charged state, respectively. The numbers next to the specimens indicate the number of runouts at a given load amplitude. For comparison, the life curves obtained by Karsch et al. [8] for the same material in treatment A state are also given. As expected, hydrogen charging reduces both lifetime and fatigue limit for both annealing states. While for treatment A specimens, the fatigue limit reduces by nearly 30%, treatment B specimens exhibit a fatigue limit drop of about 10%. When comparing both treatments in the charged state, the fatigue limit of treatment A specimens is slightly higher, while the fatigue lifetimes fall into a common scatter band. Hence, under hydrogen-influenced cyclic loading, both material states show nearly equivalent fatigue resistance and the higher initial strength of treatment A specimens degrades almost completely due to hydrogen. Notably, for treatment A specimens, hydrogen charging increases the slope of the life curve significantly. This goes along with a transition of crack initiation from the surface for non-charged specimens to cracking from near-surface oxidic agglomerates containing high amounts of Al, Ca, Si and Mg. Karsch et al. observed a similar increase in cracking from oxidic agglomerates upon hydrogen charging under push–pull loading at 20 kHz [8]. Apparently, hydrogen particularly weakens the fatigue resistance around such inclusions [29]. However, Murakami et al. found the opposite transition for 0.7C-13Cr martensitic steel, i.e., non-charged specimens initiated cracks from non-metallic inclusions while hydrogen-charged specimens showed crack initiation from the surface [4]. This suggests varying influences of hydrogen on the fatigue resistance of the surface and of inclusions depending on the inclusion type as well as on the matrix state. For SAE 51200, Karsch et al. found mainly cracking from Cr-carbides for the non-charged material [8], while we observed only surface cracking. This may either be related to the inhomogeneous rotating bending fatigue stress state featuring the highest stresses directly at the surface or to the much lower loading frequency case leading to higher plasticity in our case [30,31], particularly near the surface. Notably, the here found lifetimes of treatment A specimens in both non-charged and charged states, are significantly shorter than those reported by Karsch et al., particularly at higher stress amplitudes [8]. We assume that this is again due to the 400-fold lower test frequency in our case which gives dislocations more time to slip leading to higher plastic strain amplitudes at a given stress amplitude [32]. At lower stress amplitudes, the plastic deformation reduces and the influence of test frequency diminishes resulting in almost similar values of the fatigue limit at 10^7 cycles in both studies. For charged specimens, the lower testing frequency and thus higher plastic deformation in our case may further allow for intensified interaction between slipping dislocations and diffusing hydrogen atoms according to the HELP mechanism. Consequently, localized plasticity may increase, particularly at defects such as oxidic agglomerates or fatigue crack tips, which reduces the cycles to crack initiation and increases the fatigue crack growth rate. Interestingly, the lifetimes of charged specimens obtained by Karsch et al. scatter significantly, spanning about three orders of magnitude [8], while our results fall into a rather narrow scatter band. We assume that the higher plasticity in our experiments in combination with the HELP mechanism [25] provides the necessary plastic strain localization to induce early fatigue cracks at near-surface oxidic agglomerates of

several sizes eliminating most of the scatter. Conversely, for testing at 20 kHz, plasticity and thus plastic strain localization is less pronounced. In this case, fatigue cracks can only form at the largest oxidic agglomerates leading to considerable lifetime scatter. Consequently, fatigue lifetimes under hydrogen influence may be significantly overestimated when the prediction is based on high-frequency fatigue experiments.

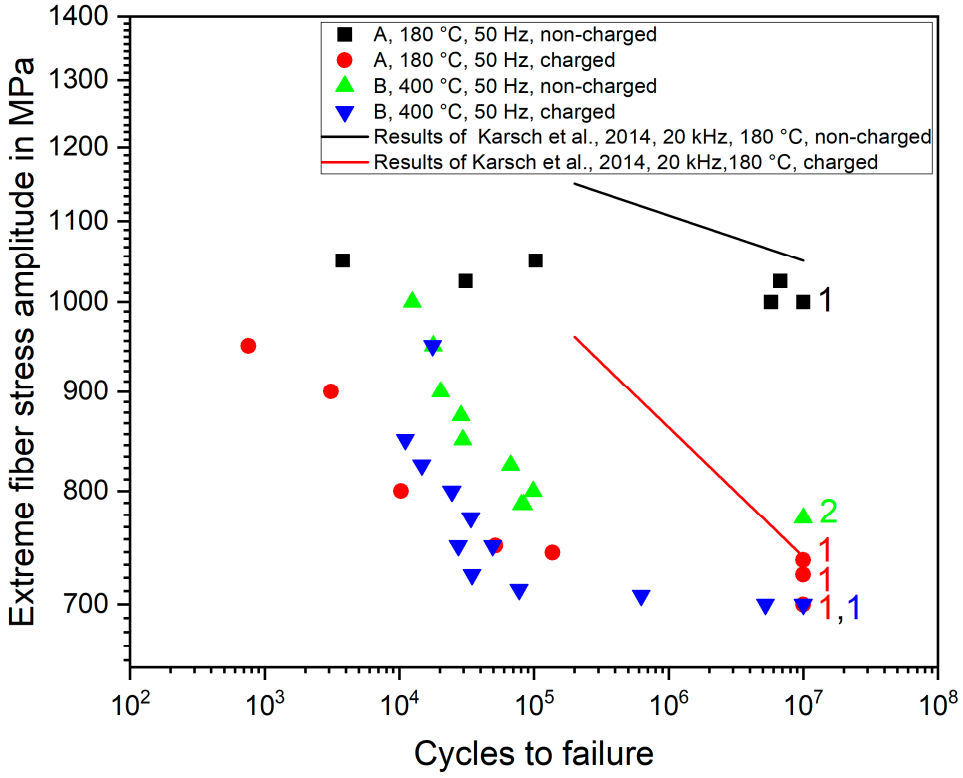

Figure 5. Fatigue lifetimes for the different material states. The lines represent mean values from the study of Karsch et al. [8], which were derived under axial tension-compression fatigue loading at a frequency of 20 kHz.

For treatment B specimens, all observed cracks initiated from the surface in both charged and non-charged states. This explains the similar slope of the life curves and indicates a higher resistance against cracking from inclusions for the softer material state upon hydrogen charging.

Figure 6 shows representative pictures of fracture surfaces of fatigue-tested specimens. The transition from fatigue fracture to forced fracture is always well visible. As can be seen from Figure 6a,b, the form of the fatigue fracture surface of treatment A specimens changes from circular to elliptic upon hydrogen charging. A similar but less pronounced trend was observed for treatment B specimens. Considering that for the typically short lifetimes of charged specimens, only the outer areas of the specimens are penetrated by hydrogen, the shape transition of the fatigue fracture surface presumably reflects the higher fatigue crack propagation rate in the hydrogen-affected near-surface volume [4,22,31]. Treatment A specimens showed in both charged and non-charged states a mixed intergranular and transgranular fatigue fracture mode, indicating that hydrogen charging did not promote grain boundary cracking (Figure 6c,d). As already discussed above, Figure 6d shows that for the hydrogen-charged treatment A state, fatigue cracks originated mainly from near-surface non-metallic agglomerates. For treatment B specimens, the dominant fatigue fracture mode was transgranular, which did not change upon hydrogen charging.

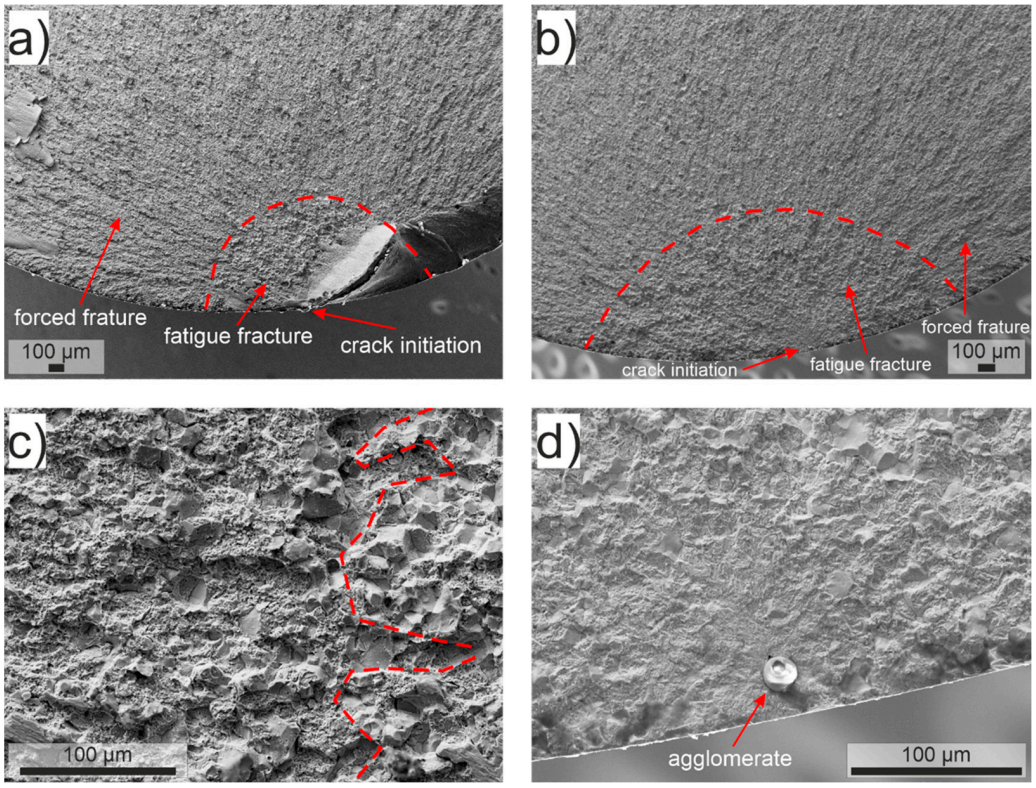

Figure 6. Typical fracture surfaces of fractured rotating bending fatigue specimens after loading. (**a**) Fatigue fracture surface of a non-charged treatment A specimen, N_f = 31,084. (**b**) Fatigue fracture surface of a charged treatment A specimen, N_f = 51,604. (**c**) Transition from fatigue fracture (**right side**) to forced fracture (**left side**) for the specimen from (**a**). The partly intergranular fracture is discernible by the facets of the former austenite grains. (**d**) Detail of the crack initiation from an agglomerate for the specimen from (**b**).

In summary, hydrogen charging did not affect the fatigue fracture mode; however, it increased the fatigue crack propagation rate in the hydrogen-affected near-surface volume. In the case of treatment A specimens, it promoted crack initiation from near-surface non-metallic agglomerates such as the mentioned oxidic particles.

Figure 7 shows how aging at room temperature and annealing at 180 °C for 2 h influences the fatigue lifetimes of hydrogen-charged treatment B specimens. Although the effective hydrogen content in the high-stressed volume decreases significantly during room temperature (see Figure 4) and reaches a level, which is similar to that of non-charged quenched and annealed material [8,25], the fatigue lifetimes remain in the scatter band of charged specimens. This is contrary to observations of Murakami and Nagata [23], who found that the fatigue lifetimes of hydrogen-charged quenched and tempered steel SCM435 recover gradually upon hydrogen effusion. Interestingly, annealing at 180 °C for 2 h restores the fatigue life of charged specimens to typical values of non-charged specimens. This implies that the hydrogen-induced material degradation is fully reversible. Hence, the charging itself does not cause damage in the form of cracks as it was found by Tiegel et al. [29], who used much more severe charging conditions. The reversibility of the hydrogen-induced lifetime reduction suggests that the damaging effect of hydrogen is based on small amounts of hydrogen in shallow traps, while the overall hydrogen content may decrease due to effusion. In the case of the treatment B material, which initiates fatigue cracks mainly from the surface, the critical shallow traps are presumably dislocation cores. When trapped at these, hydrogen atoms can promote plasticity according to the HELP mechanisms facilitating slip band formation and fatigue crack initiation [14]. We

assume that the annealing at 180 °C provides the necessary activation energy to release the hydrogen atoms from the dislocation cores and allow them to diffuse out. Consequently, the HELP mechanism does not operate anymore and the fatigue lifetime is restored to that of non-charged specimens. Szost et al. also suggested that the HELP mechanism governs HE in SAE52100 steel [26]. The fact that fatigue fracture mode does not change upon hydrogen charging supports that the HEDE mechanism does not play a decisive role here. In summary, once SAE52100 has been contaminated with hydrogen, aging and hydrogen effusion at room temperature does not improve fatigue resistance. However, an annealing treatment may restore the original fatigue resistance, as long as no damage, e.g., in the form of cracks has formed.

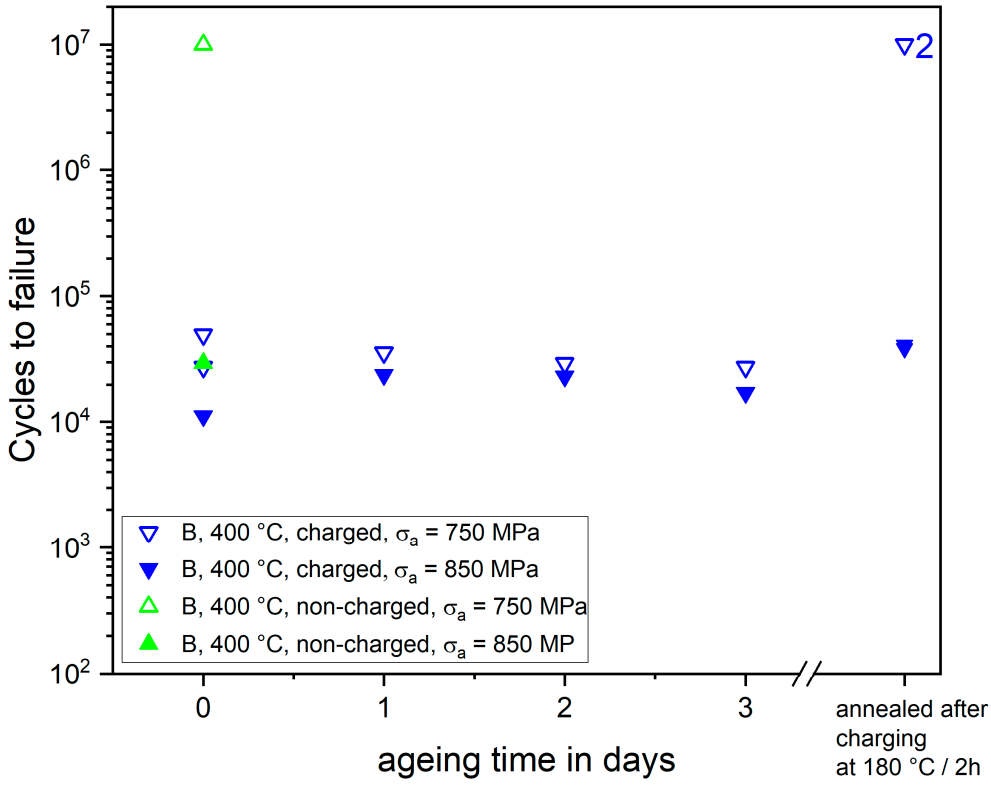

Figure 7. Influence of room temperature aging time and annealing on the fatigue lifetime at stress amplitudes of 750 and 850 MPa. Annealing restores the lifetime of hydrogen-charged samples to that of non-charged specimens. Note that there are two almost overlapping lifetime results for annealed specimens at σ_a = 850 MPa, one with 35,582 and one with 41,180 cycles to failure.

4. Conclusions

The effects of electrolytical hydrogen charging on the rotating bending fatigue behavior of the bearing steel SAE 52100 were investigated. Using two heat treatments, the material was tested in a standard hard state annealed at 180 °C and a softer state annealed at 400 °C, both with and without hydrogen charging. To study the effects of hydrogen effusion over time, hydrogen-charged samples were aged at room temperature for specific periods before fatigue testing. For both states, hydrogen charging reduces both the fatigue limit and lifetime. The fatigue limit of the hard state reduces by about 30%, while the soft state exhibits a better tolerance against hydrogen-induced degradation and loses only 10% of the original fatigue limit. Eventually, both states show similar fatigue resistances after charging. A comparison with the literature data indicates that hydrogen-induced degradation of the fatigue resistance increases with decreasing test frequency due to higher amounts of plastic deformation.

For the soft state, aging at room temperature for up to 3 days after hydrogen charging affects the resulting fatigue lifetime only insignificantly, although the hydrogen content decreases significantly due to effusion of the mobile hydrogen. Annealing for 2 h at 180 °C restores the original fatigue life indicating that for SAE 52100, hydrogen-induced material degradation can be fully reversible. We interpret this finding with a residue of hydrogen that is trapped and sessile at room temperature becoming de-trapped and mobile at 180 °C. Hence, a sufficient thermal activation is necessary to remove the damaging hydrogen from SAE 52100 steel, once it has been contaminated. The method may be also applicable to other steels.

Author Contributions: Conceptualization, S.G.; methodology, S.W.; formal analysis, J.W. and S.G.; investigation, J.W.; writing—original draft preparation, J.W. and S.G.; writing—review and editing, A.P. and S.W.; visualization, J.W.; supervision, A.P. All authors have read and agreed to the published version of the manuscript.

Funding: This research received no external funding.

Data Availability Statement: The raw data supporting the conclusions of this article will be made available by the authors on request.

Acknowledgments: The authors wish to thank N. Kandora-Mann and S. Schlabach for their help with the SEM observations.

Conflicts of Interest: The authors declare no conflict of interest.

Abbreviations

The following abbreviations are used in this manuscript:

HE	hydrogen embrittlement
HEDE	hydrogen-enhanced decohesion
HELP	hydrogen-enhanced local plasticity
SEM	scanning electron microscopy

References

1. Johnson, W.H. On Some Remarkable Changes Produced in Iron and Steel by the Action of Hydrogen in Acids. *Proc. R. Soc. Lond.* **1875**, *23*, 168–179.
2. Shakib, J.I.; Ullmaier, H.; Little, E.A.; Faulkner, R.G.; Schmilz, W.; Chung, T.E. Fatigue of DIN 1.4914 Martensitic Stainless Steel in a Hydrogen Environment. *J. Nucl. Mater.* **1994**, *212–215*, 579–583. [CrossRef]
3. Nagumo, M.; Shimura, H.; Chaya, T.; Hayashi, H.; Ochiai, I. Fatigue Damage and Its Interaction with Hydrogen in Martensitic Steels. *Mater. Sci. Eng. A* **2003**, *348*, 192–200. [CrossRef]
4. Murakami, Y.; Matsunaga, H. The Effect of Hydrogen on Fatigue Properties of Steels Used for Fuel Cell System. *Int. J. Fatigue* **2006**, *28*, 1509–1520. [CrossRef]
5. Schauer, G.; Roetting, J.; Hahn, M.; Schreijaeg, S.; Bacher-Höchst, M.; Weihe, S. Influence of Gaseous Hydrogen on Fatigue Behavior of Ferritic Stainless Steel—A Fatigue-Life Estimation. *Procedia Eng.* **2015**, *133*, 362–378. [CrossRef]
6. Aoki, Y.; Kawamoto, K.; Oda, Y.; Noguchi, H.; Higashida, K. Fatigue Characteristics of a Type 304 Austenitic Stainless Steel in Hydrogen Gas Environment. *Int. J. Fract.* **2005**, *133*, 277–288. [CrossRef]
7. Skipper, C.; Leisk, G.; Saigal, A.; Matson, D.; San Marchi, C. Effect of Internal Hydrogen on Fatigue Strength of Type 316 Stainless Steel. In *Effects of Hydrogen on Materials: Proceedings of the 2008 International Hydrogen Conference, Moran, WY, USA, 7–10 September 2008*; ASM International: Almere, The Netherlands, 2009; pp. 139–146.
8. Karsch, T.; Bomas, H.; Zoch, H.-W.; Mändl, S. Influence of Hydrogen Content and Microstructure on the Fatigue Behaviour of Steel SAE 52100 in the VHCF Regime. *Int. J. Fatigue* **2014**, *60*, 74–89. [CrossRef]
9. Barrera, O.; Bombac, D.; Chen, Y.; Daff, T.D.; Galindo-Nava, E.; Gong, P.; Haley, D.; Horton, R.; Katzarov, I.; Kermode, J.R.; et al. Understanding and Mitigating Hydrogen Embrittlement of Steels: A Review of Experimental, Modelling and Design Progress from Atomistic to Continuum. *J. Mater. Sci.* **2018**, *53*, 6251–6290. [CrossRef]
10. Dadfarnia, M.; Nagao, A.; Wang, S.; Martin, M.L.; Somerday, B.P.; Sofronis, P. Recent Advances on Hydrogen Embrittlement of Structural Materials. *Int. J. Fract.* **2015**, *196*, 223–243. [CrossRef]

11. Yang, S.; De Jesus, A.M.P.; Meng, D.; Nie, P.; Darabi, R.; Azinpour, E.; Zhu, S.-P.; Wang, Q. Very High-Cycle Fatigue Behavior of Steel in Hydrogen Environment: State of the Art Review and Challenges. *Eng. Fail. Anal.* **2024**, *166*, 108898. [CrossRef]
12. Pfeil, L.B. The Effect of Occluded Hydrogen on the Tensile Strength of Iron. *Proc. R. Soc. Lond.* **1926**, *112*, 182–195.
13. Beachem, C.D. A New Model for Hydrogen Assistant Cracking (Hydrogen "Embrittlement"). *Metall. Trans.* **1972**, *3*, 441–455.
14. Stinville, J.C.; Charpagne, M.A.; Cervellon, A.; Hemery, S.; Wang, F.; Callahan, P.G.; Valle, V.; Pollock, T.M. On the Origins of Fatigue Strength in Crystalline Metallic Materials. *Science* **2022**, *377*, 1065–1071. [CrossRef]
15. Pressouyre, G.M. A Classification of Hydrogen Traps in Steel. *Metall. Trans. A* **1979**, *10*, 1571–1573. [CrossRef]
16. Maxelon, M.; Pundt, A.; Pyckhout-Hintzen, W.; Barker, J.; Kirchheim, R. Interaction of Hydrogen and Deuterium with Dislocations in Palladium as Observed by Small Angle Neutron Scattering. *Acta Mater.* **2001**, *49*, 2625–2634. [CrossRef]
17. Pundt, A.; Kirchheim, R. HYDROGEN IN METALS: Microstructural Aspects. *Annu. Rev. Mater. Res.* **2006**, *36*, 555–608. [CrossRef]
18. Kirchheim, R.; Pundt, A. Hydrogen in Metals. In *Physical Metallurgy*; Elsevier: Amsterdam, The Netherlands, 2014; pp. 2597–2705.
19. Pundt, A.; Wagner, S. Hydrogen Interactions with Defects in Materials. *Chem. Ing. Tech.* **2024**, *96*, 182–191. [CrossRef]
20. Kuduzović, A.; Poletti, M.C.; Sommitsch, C.; Domankova, M.; Mitsche, S.; Kienreich, R. Investigations into the Delayed Fracture Susceptibility of 34CrNiMo6 Steel, and the Opportunities for Its Application in Ultra-High-Strength Bolts and Fasteners. *Mater. Sci. Eng. A* **2014**, *590*, 66–73. [CrossRef]
21. Han, B.; Binns, J.; Nedelcu, I. In Situ Detection of Hydrogen Uptake from Lubricated Rubbing Contacts. *Tribol. Online* **2016**, *11*, 450–454. [CrossRef]
22. Ogawa, T.; Hasunuma, S.; Inatomi, Y.; Yasukochi, N.; Shigeta, S. The Influence of Hydrogen on the Very High Cycle Fatigue Property and Crack Growth Characteristics of Bearing Steels. *Mech. Eng. Lett.* **2018**, *4*, 18-00134. [CrossRef]
23. Murakami, Y.; Nagata, J. Effect of Hydrogen on High Cycle Fatigue Failure of High Strength Steel, SCM435. *J. Soc. Mater. Sci. Jpn.* **2005**, *54*, 420–427.
24. Kürten, D.; Khader, I.; Kailer, A. Determining the Effective Hydrogen Diffusion Coefficient in 100Cr6. *Mater. Corros.* **2020**, *71*, 918–923. [CrossRef]
25. Sakamoto, Y.; Mantani, T. Effect of Quenching and Tempering on Diffusion of Hydrogen in Carbon Steel. *Trans. Jpn. Inst. Met.* **1976**, *17*, 743–748. [CrossRef]
26. Szost, B.A.; Rivera-Díaz-del-Castillo, P.E.J. Unveiling the Nature of Hydrogen Embrittlement in Bearing Steels Employing a New Technique. *Scr. Mater.* **2013**, *68*, 467–470. [CrossRef]
27. Salmi, S.; Rhode, M.; Jüttner, S.; Zinke, M. Hydrogen Determination in 22MnB5 Steel Grade by Use of Carrier Gas Hot Extraction Technique. *Weld. World* **2015**, *59*, 137–144. [CrossRef]
28. Richardson, A.D.; Evans, M.-H.; Wang, L.; Wood, R.J.K.; Ingram, M. Thermal Desorption Analysis of Hydrogen in Non-Hydrogen-Charged Rolling Contact Fatigue-Tested 100Cr6 Steel. *Tribol. Lett.* **2018**, *66*, 4. [CrossRef]
29. Tiegel, M.C.; Martin, M.L.; Lehmberg, A.K.; Deutges, M.; Borchers, C.; Kirchheim, R. Crack and Blister Initiation and Growth in Purified Iron Due to Hydrogen Loading. *Acta Mater.* **2016**, *115*, 24–34. [CrossRef]
30. Guennec, B.; Ueno, A.; Sakai, T.; Takanashi, M.; Itabashi, Y. Effect of the Loading Frequency on Fatigue Properties of JIS S15C Low Carbon Steel and Some Discussions Based on Micro-Plasticity Behavior. *Int. J. Fatigue* **2014**, *66*, 29–38. [CrossRef]
31. Yamabe, J.; Yoshikawa, M.; Matsunaga, H.; Matsuoka, S. Effects of Hydrogen Pressure, Test Frequency and Test Temperature on Fatigue Crack Growth Properties of Low-Carbon Steel in Gaseous Hydrogen. *Procedia Struct. Integr.* **2016**, *2*, 525–532. [CrossRef]
32. Zhao, A.; Xie, J.; Sun, C.; Lei, Z.; Hong, Y. Effects of Strength Level and Loading Frequency on Very-High-Cycle Fatigue Behavior for a Bearing Steel. *Int. J. Fatigue* **2012**, *38*, 46–56. [CrossRef]